High-Speed Force Spectroscopy Unfolds Titin at the Velocity of Molecular Dynamics Simulations

Felix Rico *et al.*

Science **342**, 741 (2013);
DOI: 10.1126/science.1239764

Science (print ISSN 0036-8075; online ISSN 1095-9203) is published weekly, except the last week in December, by the American Association for the Advancement of Science, 1200 New York Avenue NW, Washington, DC 20005.

High-Speed Force Spectroscopy Unfolds Titin at the Velocity of Molecular Dynamics Simulations

Felix Rico,[1] Laura Gonzalez,[2] Ignacio Casuso,[1] Manel Puig-Vidal,[2] Simon Scheuring[1]*

The mechanical unfolding of the muscle protein titin by atomic force microscopy was a landmark in our understanding of single-biomolecule mechanics. Molecular dynamics simulations offered atomic-level descriptions of the forced unfolding. However, experiment and simulation could not be directly compared because they differed in pulling velocity by orders of magnitude. We have developed high-speed force spectroscopy to unfold titin at velocities reached by simulation (~4 millimeters per second). We found that a small β-strand pair of an immunoglobulin domain dynamically unfolds and refolds, buffering pulling forces up to ~100 piconewtons. The distance to the unfolding transition barrier is larger than previously estimated but is in better agreement with atomistic predictions. The ability to directly compare experiment and simulation is likely to be important in studies of biomechanical processes.

Titin, a molecular spring in muscle sarcomeres, is important in striated muscle function and has been implicated in diseases such as heart failure (*1*). Titin consists of ~300 modules including immunoglobulin (Ig)–type, fibronectin III–type, and Pro-Glu-Val-Lys (PEVK) domains (*2*). Force spectroscopy (FS) unfolding of individual titin molecules, using optical tweezers (*3*, *4*) and atomic force microscopy (AFM) (*5*), opened a new research field relating protein mechanics, structure, and folding. AFM force-extension curves revealed sawtooth-like patterns (periodicity 25 to 28 nm) that indicated unfolding of individual Ig-like domains (*5*). Combinations of AFM experiments with steered molecular dynamics (SMD) simulations enriched atomic-level descriptions (*6*–*8*) of receptor-ligand binding (*9*, *10*) and forced protein unfolding (*5*). Forced unfolding (pulling speed 0.3 to 0.5 μm/s) of titin I91 concatemers (*8*, *11*, *12*) resulted in extension of each domain by ~0.7 nm, which correlated with the separation of antiparallel β strands A and B observed in SMD simulations (*8*, *11*). Subsequent rupture of the A′-G β-strand pair led to complete domain unfolding (*11*, *13*, *14*). However, a velocity difference of about six orders of magnitude prevented direct comparison of SMD with FS. Indeed, simulations resulted in unfolding forces of ~1 nN, nearly an order of magnitude greater than experimental values (*11*, *12*). Improved computational abilities have allowed simulations that unfolded I91 at 2800 μm/s (still faster than experiment by ~2.5 orders of magnitude), reporting forces of ~500 pN (*15*).

High-speed AFM [HS-AFM (*16*)] allows imaging biomolecules at video rate (*17*–*19*) through miniaturization of piezoelectric elements and the cantilever (*20*). We developed an analogous technique, high-speed FS (HS-FS), with short cantilevers (*21*) that allowed titin molecules to be pulled at speeds up to ~4000 μm/s. This is faster than conventional AFM by ~2.5 orders of magnitude and reaches current limits for SMD simulations.

Our HS-FS setup consists of a miniature piezoelectric actuator and a short cantilever with small viscous damping (0.035 pN μm^{-1} s^{-1}) (Fig. 1A and figs. S1 and S2). Titin I91 concatemers were unfolded by HS-FS at pulling velocities ranging over six orders of magnitude, from 0.0097 to 3870 μm/s. Only force curves with at least three sawtooth-like unfolding peaks were analyzed (*22*) (Fig. 1B and fig. S3). As reported in (*5*, *23*), unfolding forces increased with pulling velocity (Fig. 2A). At slow velocities, HS-FS unfolding forces were in excellent agreement with conventional FS (Fig. 2B). At pulling velocities higher than previously (>100 μm/s), unfolding forces followed a steeper slope that reached values greater than 500 pN and overlapped those obtained by simulations (Fig. 2B). Variations in the slope of the plot of mean rupture forces versus the logarithm of the velocity (force spectrum) have been observed for receptor-ligand interactions (*24*–*26*) but have rarely been documented for protein unfolding (*27*), probably because of the limited range of accessible pulling rates.

The microscopic model developed by Hummer and Szabo (*26*, *28*) allowed us to fit the wide range of pulling velocities and describes well the nonlinear upturn in the dynamic force spectrum (*26*, *28*) (Fig. 2B and supplementary materials). According to this theory, at moderate velocities, unfolding is dominated by the pulling rate and stochastic fluctuations (i.e., spontaneous unfolding of the domain under a given force). At high velocities, stochastic fluctuations of the protein along the unfolding pathway become irrelevant and the unfolding process becomes deterministic (*28*), because the protein is pulled so fast that it has no time to explore its energy landscape.

The slope in the dynamic force spectrum is related to the position of the energy barrier;

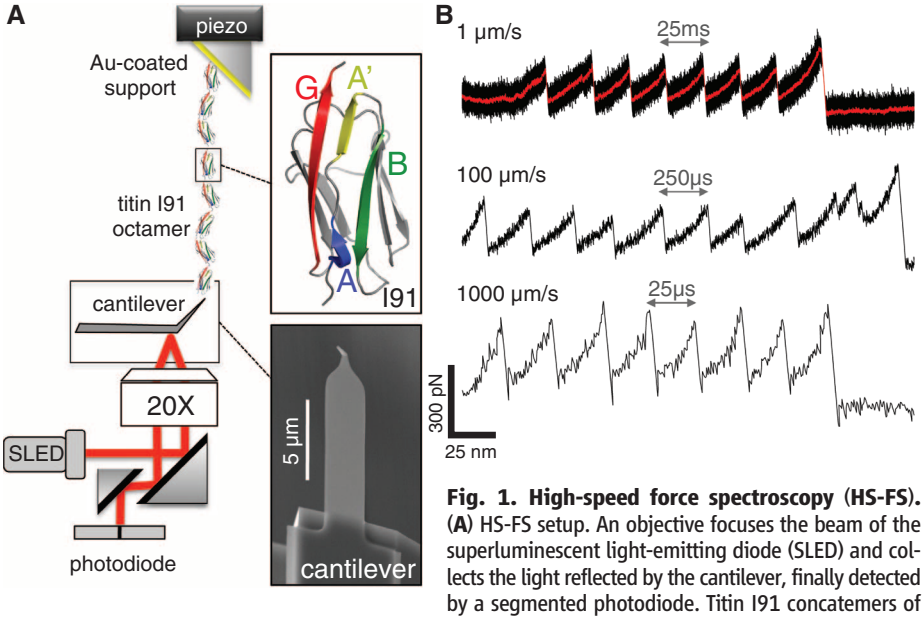

Fig. 1. High-speed force spectroscopy (HS-FS). (**A**) HS-FS setup. An objective focuses the beam of the superluminescent light-emitting diode (SLED) and collects the light reflected by the cantilever, finally detected by a segmented photodiode. Titin I91 concatemers of eight domains are immobilized on a tilted gold-coated surface via C-terminal cysteines. They are pulled by their N-terminal histidine tag with a nickel-coated tip at the end of a short cantilever. Tilting the sample surface further reduces hydrodynamic forces. Top inset shows a titin I91 domain (PDB ID: 1TIT) with relevant β strands colored in blue (A), yellow (A′), green (B), and red (G). Bottom inset shows a scanning electron micrograph of a short cantilever. (**B**) Force-extension curves acquired at three different retraction velocities: 1, 100, and 1000 μm/s. The 1 μm/s curve is moving average–filtered (red trace, 65-μs time window). Times to unfold a single I91 domain are indicated by arrows.

[1]U1006 INSERM, Aix-Marseille Université, Parc Scientifique et Technologique de Luminy, 163 avenue de Luminy, 13009 Marseille, France. [2]Bioelectronics Group, Department of Electronics, Universitat de Barcelona, c/ Marti Franques 1, 08028 Barcelona, Spain.

*Corresponding author. E-mail: simon.scheuring@inserm.fr

therefore, the slope upturn at high velocities corresponds to a shift of the barrier closer to the native state. From our data, the regime transition occurs at experimental velocities of ~1000 μm/s and a critical force of ~350 pN (supplementary materials). Our fastest experiment at 3870 μm/s is situated at the beginning of the deterministic regime, whereas most of the HS-FS data points characterize the transition from the stochastic regime to the deterministic regime (Fig. 2B). SMD simulations at much higher velocities (>>1000 μm/s) have generally been carried out in this deterministic regime. Although SMD simulation–derived forces are in agreement with our fastest pulling data, the theoretically predicted trend deviates from simulations at velocities of $>10^4$ μm/s. These deviations may be explained by slight differences in the simulated conditions (e.g., temperature) or by the simple cusp shape of the potential in the theory. More refined theories may be necessary to describe the unfolding at very high velocities. The model fit results in an energy landscape where the unfolding transition barrier (x_β) is located at 0.89 nm and the molecular elasticity (k_m) is 376 pN/nm, leading to an unfolding barrier height (ΔG) of $36k_BT$ and a spontaneous unfolding rate k_0 of 2×10^{-10} s^{-1} (fig. S4). Similar values were obtained by fitting a unified model valid for different potential shapes (*28*) to the unfolding forces at velocities of ≤100 μm/s; this suggested that the reported parameters are independent of the potential shape (fig. S6). Our barrier position (0.89 nm) is larger than previous experimental estimates [0.25 nm (*23*); 0.30 nm (*5*)] but is in better agreement with the distance (1.1 to 1.4 nm) at which the secondary structure of I91 breaks in simulations (*8*, *15*). The relatively narrow range of experimental velocities in former FS experiments did not show an upturn in the force spectra and hence justified the Bell-Evans assumption of a fixed distance to the transition barrier under force. Our experiments at higher velocities show that this assumption is not valid. Furthermore, the data allowed us to estimate a diffusion coefficient of the protein along the reaction coordinate of the free energy landscape $D \approx 4 \times 10^3$ nm^2/s (supplementary materials). This is orders of magnitude slower than diffusion coefficients of proteins in solution ($\sim 10^8$ nm^2/s) (*29*).

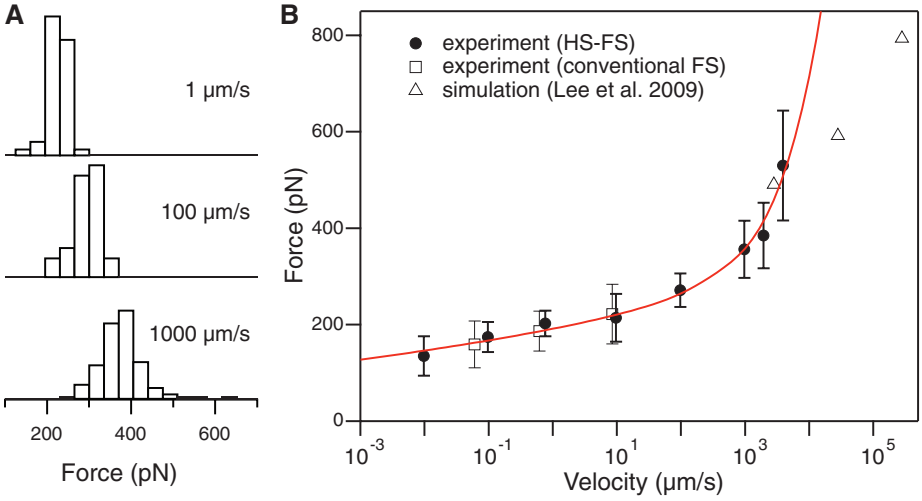

Fig. 2. High-speed dynamic force spectrum of titin I91. (**A**) Unfolding force histograms of the 1, 100, and 1000 μm/s retraction velocity experiments. (**B**) Average unfolding forces versus retraction velocity obtained using HS-FS, conventional FS (error bars denote SD), and steered molecular dynamics simulations [data from Lee *et al*. (*15*)]. Solid red line is the fit to the entire dynamic range of HS-FS with the full microscopic model (*26*) with fitting parameters (±SD) of $x_\beta = 0.89 \pm 0.05$ nm, $D = 3925 \pm 183$ nm^2/s, and $k_m = 376 \pm 28$ pN/nm.

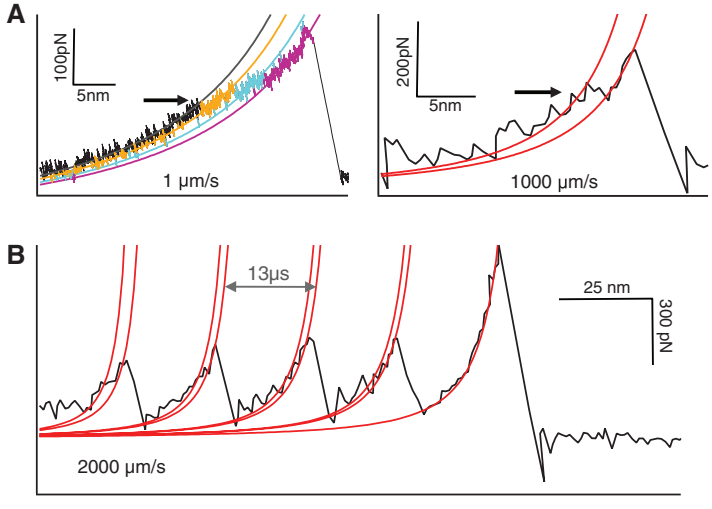

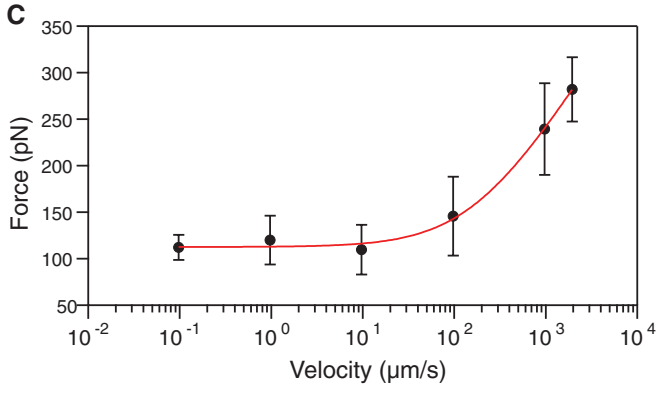

Fig. 3. High-speed force spectroscopy of unfolding intermediate. (**A**) Left: Force-extension trace at 1 μm/s (moving average–filtered with 65-μs time window) showing the intermediate unfolding state "hump" (arrow) separating antiparallel β strands A and B. Cantilever fluctuations above the noise level of the trace are interpreted as hopping between intermediate states of the remaining folded domains (see fig. S5). Colored lines are worm-like chain (WLC) model fits. Right: Force-extension trace (black line) at 1000 μm/s showing the intermediate unfolding state "hump" (arrow). Red lines are the best fits of the WLC model to the hump and complete unfolding peaks. The difference between the contour lengths is consistent with a separation of $n \times 0.7$ nm of each A-B β-strand pair of the remaining folded domains (*11*). (**B**) Force-extension curve at 2000 μm/s showing unfolding of four I91 domains. Red lines are WLC fits to the "hump" and complete unfolding peaks. The contour length distance difference between the "hump" and the complete unfolding decreases with the decreasing number of remaining folded domains. (**C**) Dynamic force spectrum of the intermediate unfolding state. Solid red line is the best fit of the model developed by Friddle *et al*. (*33*) to the experimental data with fitting parameters (±SD) $x_t = 0.060 \pm 0.004$ nm, $f_{eq} = 113 \pm 1$ pN, and $k_{NI} = 6959^{+1398}_{-990}$ s^{-1}.

Slow diffusion has been interpreted as a result of cantilever viscous damping (*30*) or by local minima along the unfolding pathway (*31*). Given the much smaller damping coefficient of the cantilevers used here, our data support the hypothesis that roughness in the free energy landscape slows unfolding. Although our estimated barrier height ($36.4k_BT$) is similar to that measured from chemical unfolding ($37k_BT$), the intrinsic unfolding rate (2×10^{-10} s^{-1}) is much slower than estimates from FS at slow pulling velocity (3.3×10^{-4} s^{-1}) and chemical unfolding (4.9×10^{-4} s^{-1}) (*23*). The fast intrinsic dissociation rate from slow FS and Bell-Evans analysis suggests an oversimplified view of forced unfolding, whereas chemical unfolding explores unrestricted unfolding pathways different from the physiologically relevant directional unfolding during muscle relaxation. Indeed, our slow k_0 suggests that the titin I91 domains unfold only very rarely at the estimated physiological forces (~5 pN) acting on distal titin Ig domains (*32*).

The use of short cantilevers with fast response (response time $\tau_c \approx 0.7$ μs; Fig. 1) allowed us not only to pull fast but also at conventional velocities (10 to 1000 nm/s) with microsecond time resolution. This response time is almost three orders of magnitude shorter than that of conventional cantilevers and allowed estimation of a lower limit for the relaxation time of the unfolded polypeptide chain (<2 μs; fig. S3). Before complete domain unfolding, an intermediate state has previously been documented by the so-called "hump" in force curves (Fig. 3A, arrows). This intermediate state is characterized by a force drop in the stretching regime (Fig. 3A, arrows), caused by the separation of the A-B β-strand pair as revealed by simulations (*11*, *12*). HS-FS measurements show separation of the A-B β-strand pair in several domains within 1 μs (Fig. 3B, first peak). Additionally, at high retraction speeds (>1 mm/s), the first domain as well as consecutive domains presented a "hump" before unfolding. The percentage of domains displaying intermediate unfolding decreased from ~95% at the lowest velocities to ~40% at the highest velocities. At 2 mm/s, the time between domain unfolding was ~10 μs (Fig. 3B). Thus, this short time lapse after the unfolding of the preceding domain is sufficient for domains to refold into their native state. This result allows us to set the lower limit for the refolding rate from the intermediate to the native state to at least ~10^5 s^{-1}, much faster than previous estimates (25 s^{-1}) (*11*).

We analyzed the intermediate unfolding state up to 2000 μm/s; beyond this velocity, it is difficult to assess an accurate measurement (Fig. 3 and fig. S3). At conventional pulling velocities, the average unfolding forces to the intermediate state are independent of pulling rate. At velocities faster than ~100 μm/s, average "hump" forces increase drastically, reaching values up to ~300 pN (Fig. 3C), consistent with "hump" forces observed in simulations (*15*). The slow pulling regime (<100 μm/s) is dominated by near-equilibrium unfolding and refolding of the A-B β-strand pair and defines the equilibrium force (Fig. 3A). At higher velocities, refolding of the A-B β-strand pair is negligible and the structure unfolds stochastically at forces that increase with the logarithm of the pulling rate (*33*) (Fig. 3C and supplementary materials). The model fitted our results with an unfolding rate at zero force from native to intermediate (k_{NI}^0) of 7×10^3 s^{-1}, an even faster folding rate at zero force from intermediate to native (k_{IN}^0) of 4×10^5 s^{-1}, a distance x_t to the transition barrier of only 0.06 nm, and an equilibrium force f_{eq} of 113 pN where $k_{NI}^0 = k_{IN}^0 = 2.8 \times 10^4$ s^{-1}. This results in an equilibrium free energy difference between the native and intermediate states of ~$4.1k_BT$, in agreement with the expected energy of three hydrogen bonds.

Although the absolute values of the calculated rates should be interpreted with care, the refolding rate of 4×10^5 s^{-1} is in excellent agreement with the lower limit (~10^5 s^{-1}) determined directly through observation of reformed A-B β-strand pairs in high-velocity unfolding traces (fig. S3). This suggests fast dynamic equilibrium of unfolding and refolding of β strand pair A and B at pulling forces up to ~100 pN, probably maintained by the antiparallel structure. This behavior has been observed in SMD runs (*12*, *15*). Furthermore, a recent computational small protein folding study reported that an antiparallel three–β-strand domain required an average of 21 μs to fold (*34*). This suggests a novel insight into the A-B β-strand pair and perhaps into short β folds in general: unfolding at fast rates, and refolding at even faster rates, as a feature of their structural equilibrium.

The combination of SMD with experimental FS has been important in understanding protein unfolding and mechanical stability. Our HS-FS methodology provides pulling velocities over six orders of magnitude and provides microsecond time resolution, achieving rates comparable to SMD simulations and thus allowing direct comparison of experimental and simulated unfolding forces. We expect that the now accessible dynamic range of HS-FS will stimulate the development of novel theories. Our results imply detailed mechanisms of the various steps during titin I91 unfolding: At zero and moderate forces, the protein fluctuates between the native and intermediate states. Under increasing force, only the intermediate state is populated. Thus, the tethered molecule reveals slow diffusion along the unfolding pathway, which, in combination with a high energy barrier, results in high mechanical stability. Direct comparison of FS and SMD simulations will likely provide new insights into other important biological processes such as lipid membrane dynamics (*35*) and receptor-ligand unbinding (*7*, *9*).

References and Notes

1. D. S. Herman *et al.*, *N. Engl. J. Med.* **366**, 619–628 (2012).
2. K. Maruyama, S. Matsubara, R. Natori, Y. Nonomura, S. Kimura, *J. Biochem.* **82**, 317–337 (1977).
3. M. S. Z. Kellermayer, S. B. Smith, H. L. Granzier, C. Bustamante, *Science* **276**, 1112–1116 (1997).
4. L. Tskhovrebova, J. Trinick, J. A. Sleep, R. M. Simmons, *Nature* **387**, 308–312 (1997).
5. M. Rief, M. Gautel, F. Oesterhelt, J. M. Fernandez, H. E. Gaub, *Science* **276**, 1109–1112 (1997).
6. H. Grubmüller, B. Heymann, P. Tavan, *Science* **271**, 997 (1996).
7. S. Izrailev, S. Stepaniants, M. Balsera, Y. Oono, K. Schulten, *Biophys. J.* **72**, 1568–1581 (1997).
8. H. Lu, B. Isralewitz, A. Krammer, V. Vogel, K. Schulten, *Biophys. J.* **75**, 662–671 (1998).
9. E. L. Florin, V. T. Moy, H. E. Gaub, *Science* **264**, 415–417 (1994).
10. G. U. Lee, L. A. Chrisey, R. J. Colton, *Science* **266**, 771–773 (1994).
11. P. E. Marszalek *et al.*, *Nature* **402**, 100–103 (1999).
12. H. Lu, K. Schulten, *Biophys. J.* **79**, 51–65 (2000).
13. S. B. Fowler *et al.*, *J. Mol. Biol.* **322**, 841–849 (2002).
14. R. B. Best *et al.*, *J. Mol. Biol.* **330**, 867–877 (2003).
15. E. H. Lee, J. Hsin, M. Sotomayor, G. Comellas, K. Schulten, *Structure* **17**, 1295–1306 (2009).
16. T. Ando *et al.*, *Proc. Natl. Acad. Sci. U.S.A.* **98**, 12468–12472 (2001).
17. T. Uchihashi, R. Iino, T. Ando, H. Noji, *Science* **333**, 755–758 (2011).
18. N. Kodera, D. Yamamoto, R. Ishikawa, T. Ando, *Nature* **468**, 72–76 (2010).
19. I. Casuso *et al.*, *Nat. Nanotechnol.* **7**, 525–529 (2012).
20. T. Ando, T. Uchihashi, T. Fukuma, *Prog. Surf. Sci.* **83**, 337–437 (2008).
21. M. B. Viani *et al.*, *J. Appl. Phys.* **86**, 2258 (1999).
22. R. B. Best *et al.*, *Anal. Chim. Acta* **479**, 87–105 (2003).
23. M. Carrion-Vazquez *et al.*, *Proc. Natl. Acad. Sci. U.S.A.* **96**, 3694–3699 (1999).
24. R. Merkel, P. Nassoy, A. Leung, K. Ritchie, E. Evans, *Nature* **397**, 50–53 (1999).
25. X. H. Zhang, E. Wojcikiewicz, V. T. Moy, *Biophys. J.* **83**, 2270–2279 (2002).
26. G. Hummer, A. Szabo, *Biophys. J.* **85**, 5–15 (2003).
27. Z. T. Yew, M. Schlierf, M. Rief, E. Paci, *Phys. Rev. E* **81**, 031923 (2010).
28. O. K. Dudko, G. Hummer, A. Szabo, *Phys. Rev. Lett.* **96**, 108101 (2006).
29. L. J. Lapidus, W. A. Eaton, J. Hofrichter, *Proc. Natl. Acad. Sci. U.S.A.* **97**, 7220–7225 (2000).
30. R. Berkovich *et al.*, *Proc. Natl. Acad. Sci. U.S.A.* **109**, 14416–14421 (2012).
31. H. Lannon, J. S. Haghpanah, J. K. Montclare, E. Vanden-Eijnden, J. Brujic, *Phys. Rev. Lett.* **110**, 128301 (2013).
32. H. Li *et al.*, *Nature* **418**, 998–1002 (2002).
33. R. W. Friddle, A. Noy, J. J. De Yoreo, *Proc. Natl. Acad. Sci. U.S.A.* **109**, 13573–13578 (2012).
34. K. Lindorff-Larsen, S. Piana, R. O. Dror, D. E. Shaw, *Science* **334**, 517–520 (2011).
35. L. Redondo-Morata, M. I. Giannotti, F. Sanz, *Langmuir* **28**, 6403–6410 (2012).

Acknowledgments: We thank A. Sastre and J. Otero for helpful discussions. Supported by European Research Council starting grant 310080 and Agence National de la Recherche grant ANR-12-BS10-009-01. L.G. was a recipient of travel grants (FPI grant BES-2010-031186 from the Spanish Ministerio de Economía y Competitividad and STSM COST Action TD1002-10006).

Supplementary Materials

www.sciencemag.org/content/342/6159/741/suppl/DC1
Materials and Methods
Supplementary Text
Figs. S1 to S6
References (*36*–*39*)

29 April 2013; accepted 30 September 2013
10.1126/science.1239764